

1 **Hemap: An interactive online resource for characterizing molecular phenotypes**
2 **across hematologic malignancies**

3 Petri Pölönen¹⁺, Juha Mehtonen¹⁺, Jake Lin^{2,3+}, Thomas Liuksiala^{2,4+}, Sergei Häyrynen²,
4 Susanna Teppo⁴, Artturi Mäkinen^{4,5}, Ashwini Kumar³, Disha Malani³, Virva Pohjolainen⁵,
5 Kimmo Porkka⁶, Caroline A. Heckman³, Patrick May⁷, Ville Hautamäki⁸, Kirsi J. Granberg²,
6 Olli Lohi⁴, Matti Nykter^{2*}, and Merja Heinäniemi^{1*}

7

8 ¹Institute of Biomedicine, School of Medicine, University of Eastern Finland, Kuopio, Finland

9 ²Faculty of Medicine and Health Technology, Tampere University, Tampere, Finland

10 ³Institute for Molecular Medicine Finland FIMM, Helsinki Institute of Life Science, University of
11 Helsinki, Helsinki, Finland

12 ⁴Tampere Center for Child Health Research, Tampere University and Tampere University Hospital,
13 Tampere, Finland

14 ⁵Tampere University Hospital, Fimlab Laboratories, Tampere, Finland

15 ⁶Hematology Research Unit Helsinki, University of Helsinki and Helsinki University Central Hospital
16 Cancer Center, Department of Hematology, Helsinki, Finland

17 ⁷Luxembourg Center for Systems Biomedicine, University of Luxembourg, Esch-Belval, Luxembourg

18 ⁸School of Computing, University of Eastern Finland, Kuopio, Finland

19 + equal contribution * co-corresponding authors

20

21 Conflict of interest statement: CH has research funding from Celgene, Novartis and Orion
22 Pharma unrelated to this study.

23

24 Word count: 5849, Number of figures: 5, Number of Tables: 1. The supplementary material
25 consists of supplemental methods and Supplementary display items; 5 figures and 6 tables
26 with their legends.

27

28 Running title: Organizing molecular diversity of hematologic malignancies

29

30 Corresponding authors:

31 Associate Prof. Merja Heinäniemi

32 School of Medicine, University of Eastern Finland, Kuopio, Finland

33 Tel. +358 41 4305724

34 Email: merja.heinaniemi@uef.fi

35

36 Prof. Matti Nykter

Doc. Olli Lohi, MD

37 Faculty of Medicine and Health Technology

Faculty of Medicine and Health Technology

38 Tampere University, Tampere, Finland

Tampere University, Tampere, Finland

39 Tel. +358 40 5267884

Tel. +358 50 318 6254

40 Email: matti.nykter@uta.fi

Email: olli.lohi@uta.fi

41

42

43

Abstract

44

45 Large collections of genome-wide data can facilitate the characterization of disease states
46 and subtypes, permitting pan-cancer analysis of molecular phenotypes and evaluation of
47 disease context for new therapeutic approaches. We analyzed 9,544 transcriptomes from
48 more than 30 hematologic malignancies, normal blood cell types, and cell lines, and showed
49 that disease types could be stratified in a data-driven manner. We then identified cluster-
50 specific pathway activity, new biomarkers and in silico drug target prioritization through
51 interrogation of drug target databases. Using known vulnerabilities and available drug
52 screens, we highlighted the importance of integrating molecular phenotype with drug target
53 expression for in silico prediction of drug responsiveness. Our analysis implicated *BCL2*
54 expression level as an important indicator of venetoclax responsiveness and provided a
55 rationale for its targeting in specific leukemia subtypes and multiple myeloma, linked several
56 polycomb group proteins that could be targeted by small molecules (SFMBT1, CBX7 and
57 EZH1) with CLL, and supported *CDK6* as a disease-specific target in AML. Through
58 integration with proteomics data, we characterized target protein expression for pre-B
59 leukemia immunotherapy candidates, including DPEP1. These molecular data can be
60 explored using our publicly available interactive resource, Hemap, for expediting therapeutic
61 innovations in hematologic malignancies.

62

63

Significance

64

65 This study describes a data resource for researching derailed cellular pathways and
66 candidate drug targets across hematological malignancies.

67

68

Introduction

69

70 Gene expression profiles facilitate genome-wide analyses that can stratify patient subtypes
71 and identify the activity patterns of various cellular pathways under different biological
72 conditions (1-2). Even though a large number of studies have characterized hematologic
73 malignancies and normal blood cell types at genome-wide level since the introduction of
74 microarray technology, most include only tens to hundreds of samples and focus on one
75 disease. Thus, understanding the complete heterogeneity and similarity of diseases states

76 and their subtypes remains an open challenge. Moreover, many hematologic malignancies
77 are rare on the population level, necessitating collecting data across study cohorts.

78

79 Hematological malignancies include acute and chronic leukemias of myeloid and lymphoid
80 lineage, B-, T- and NK cell lymphomas, and multiple myeloma (MM), and a number of
81 premalignant conditions such as myelodysplastic syndrome (MDS), and myeloproliferative
82 neoplasms (MPN). These diseases have highly variable genetic features, unique clinical
83 courses, and varying therapeutic approaches. There is also a marked difference in
84 prevalence, genetic background and prognosis between adult and pediatric blood cancers.
85 In children, acute lymphoblastic leukemia (ALL) is the most common hematological
86 malignancy, while in adults, non-Hodgkin lymphomas (NHL), followed by MM, chronic
87 lymphocytic leukemia (CLL), and acute myeloid leukemia (AML) are the most common.
88 Treatment is moving towards increased utilization of targeted therapies in combination with
89 traditional chemotherapies. Targeted therapies include tyrosine kinase inhibitors such as
90 those developed against BCR-ABL fusion found in CML and some ALL cases, or antibody
91 therapies including CD38-targeting in MM, and engineered CAR-T cells recognizing cell
92 surface CD19 or CD22 antigens in relapsed ALL and NHL (3-5). Yet, current therapies to
93 treat hematologic malignancies rely heavily on drugs that target DNA metabolism in actively
94 proliferating cells or intracellular signaling events that are involved in proliferation (6).
95 Although these drugs have markedly improved progression-free survival, redundancy in
96 signaling and the failure to eradicate quiescent cells (7) can facilitate the rapid development
97 of therapy resistance. Testing a wider portfolio of new drug targets, or repurposing drugs
98 with established clinical indications represent promising strategies (6-7). Molecular profile
99 guided approaches hold promise to improve the efficiency of this process (8).

100

101 We present here a resource that organizes samples from cancer patients, healthy donors
102 and those at pre-malignant stages for comparative analysis based on both curated
103 annotations and data-driven clustering of molecular phenotypes. This hematologic pan-
104 cancer analysis permits the identification of clinically relevant molecular features and the
105 exploration of new drug targeting approaches across the disease hierarchy. The data and
106 analysis tools are made available as an interactive online resource, Hemap,
107 <http://hemap.uta.fi/> that synthesizes the curated genome-wide data across different disease
108 subtypes.

109
110
111
112

Materials and Methods

113 **Dataset retrieval and extraction of sample annotation data**

114 Transcriptome datasets for Hemap were retrieved from the NCBI Gene Expression Omnibus
115 (GEO) database (9) and represent samples hybridized to hgu133Plus2 genome-wide
116 microarrays. The meta-data were retrieved based on matching disease ontology terms for
117 hematologic malignancies against sample annotations (R/Bioconductor GEOmetadb
118 package, “gsm” and “gse” tables), followed by manual curation, resulting in 10,470 samples.
119 Refer to Methods Supplement for details. Eight leukemia types, 8 B-cell lymphoma types, 7
120 T/NK lymphomas, multiple myeloma and 4 proliferative disorders are represented by primary
121 patient samples, while in total 36 disease types are included considering also their sub-
122 categories and cell line data (**Tables S1** and **S2**).

123

124 **Data preprocessing and quality control**

125 Samples with a median of raw probe intensity distribution deviating more than 1.5 in log2-
126 scale from the median of all medians were deemed outliers and filtered out as well as those
127 with an interquartile range (IQR) deviating more than 0.75 from the median of IQRs. Finally,
128 duplicate samples, as well as all disease types with less than 3 samples (and samples
129 assigned to these), were removed, resulting in 9,544 samples that were processed using the
130 RMA probe summarization algorithm (10) with probe mapping to Entrez Gene IDs (from
131 BrainArray version 18.0.0, ENTREZG). Finally, we employed the bias-correction method (11)
132 to correct for any remaining technical differences (**Fig. S1**). BeatAML (12) clinical and
133 mutation data was obtained from source data file 41586_2018_623_MOESM3_ESM.xlsx.
134 RNAseq counts were obtained from the authors. Genes with over 1 cpm expression in over
135 1 % of the samples were kept. Data was normalized using limma voom and quantile
136 normalization.

137

138 **Dimensionality reduction**

139 Dimensionality reduction methods are unsupervised methods that use measures of
140 (dis)similarity and an optimization strategy to return as output sample coordinates in a lower
141 dimension. Metrics of continuity, trustworthiness and k-NN error were used to assess how

142 well the visualization in 2D preserved their relative placement in the original coordinate
143 space. We tested Gaussian Process Latent Variable Model (GPLVM) (13), Locally Linear
144 Embedding (LLE) (14), Principal Component Analysis (PCA) (15), Probabilistic Principal
145 Component Analysis (PPCA) (16), Sammon Mapping (SM) (17) and t-Distributed Stochastic
146 Neighbor Embedding (t-SNE) (18) (see Methods Supplement for parameters). Comparison
147 of the different methods encouraged the selection of t-SNE maps, specifically the Barnes-
148 Hut approximated version of t-SNE implementation (BH-SNE) (19). In final analysis 15%
149 genes with highest variance were used in construction of t-SNE maps (see (20) for
150 justification).

151

152 **Assignment of cluster centers on t-SNE maps**

153 Kernel density-based clustering algorithm (mean-shift clustering with bandwidth parameter
154 set to 2.5, LPCM-package in R), was used to cluster the data following the dimensionality
155 reduction. This method allows the discovery of sample sets which share similar features
156 without having to pre-specify the number of clusters. The term “cluster” is used in the text to
157 refer to this computational clustering result, and the term “group” is used in context of visual
158 examination. Pairwise statistical analysis between different sample features and clusters
159 was performed as in (21), based on Spearman correlation and the Bonferroni method for
160 multiple hypothesis testing correction (see Methods Supplement for details).

161

162 **Discretizing gene expression with mixture models**

163 Microarray hybridization generates background signal, which we would like to distinguish
164 from real expression signal. The large sample size of Hemap was leveraged for fitting gene-
165 specific models to cluster the gene expression in two components (expressed and not
166 detected, denoted by 1 and -1, respectively). Gaussian finite mixture models were fitted by
167 expectation-maximization algorithm (R package mclust version 4.3). If the uncertainty value
168 from the model was more than 0.1, we assigned a value of 0 to denote low level.
169 Additionally, each log₂ expression value lower than 4 was assigned a value -1 and values
170 higher than 10 a value of 1. This was done to assure minimal amount of misclassifications of
171 data samples to wrong components. The model was chosen by fitting both equal and
172 variable variance models and ultimately choosing the model which achieved a higher
173 Bayesian Information Criterion (BIC) to avoid overfitting. For drug target analysis, we utilized
174 an adjustment for genes where background distribution was not found (gene is always
175 expressed), or if over 90% of the samples had uncertain expression based on the model
176 classification. Expressed state was assigned when >60% of the uncertain samples had
177 expression above 6. Not detected status was re-evaluated similarly (60% at level below 6).

178

179 **Gene set analysis**

180 The pathway and gene set enrichment analysis available in the Hemap resource was
181 generated based on gene sets retrieved from MsigDB v5.0 (22) (molecular signatures),
182 Wikipathways (06.2015) (23), Recon 1 (24) (metabolic pathways), Pathway Commons 7 (25)
183 and DSigDB v1.0 (26) (drug targets). Gene sets were limited to contain between 5 to 500
184 expressed genes (as defined above) per gene set, resulting in 19,680 gene sets that were
185 evaluated across the dataset. The gene set variation analysis (GSVA) (27), GSVA package
186 1.13.0 in R, was used to calculate gene set enrichment scores (positive for increased and
187 negative for decreased expression) for each sample (parameters $mx.diff=F$, $\tau=0.25$,
188 $rnaseq=F$). Significance was evaluated based on empirical *P*-values calculated using 1000
189 random permutations of genes within the gene set, separately for gene set sizes 5-20, 25,
190 30, 40, 50, 75, 100, 200, 300, 400, and 500 to correct for differences in gene set sizes.
191 Hypergeometric test was used to calculate enrichment of significant scores in a specific
192 cluster.

193

194 **Data sources used for evaluating drug targeting approaches**

195 Drugs in clinical trials for leukemias, lymphomas or multiple myeloma were obtained from
196 ClinicalTrials.gov (accessed March 7th, 2018) maintained by the U.S. National Institutes of
197 Health, including ongoing and terminated trials. Leukemia clinical trials were further sorted to
198 those with clinical indication associated with AML, pre-B-ALL, CML, CLL or multiple
199 leukemia types. Drugs in use based on approved status in Finland were provided by the
200 Finnish Pharmaceutical Information Centre Ltd and drugs approved by the Food and Drug
201 Administration (FDA) for leukemia, lymphoma and myeloma were queried from FDA website
202 (fda.gov – Drugs – Information on Drugs) (**Table S3**). A table of gene level details for each
203 drug was obtained from DSigDB (26) (DSigDBv1.0 Detailed.txt) and integrated to Hemap *in*
204 *silico* drug screening analysis. The list of drugs targeting epigenetic modifiers is based on
205 the gene list with 124 genes available from ChEMBL_20 Target Classification Hierarchy (28)
206 (**Table S4**). Analysis using TTD (Therapeutics Targets Database) (29), DGIdb3.0 (30) for
207 FDA approved drugs across a wider disease context (31) as a source database was based
208 on a total of 11,373 unique drugs and 1270 unique genes. Drugs in use and in clinical trial
209 included high confidence targets that were reported in several databases or had an
210 associated Pubmed identifier. A surface marker gene list with total of 996 genes was
211 obtained from Cell Surface Protein Atlas (32) to evaluate putative novel immunotherapy
212 targets.

213

214 **Drug target *in silico* analysis in hierarchical manner**

215 A disease hierarchy: 1. All disease samples; 2. disease combinations; 3. leukemia,
216 lymphoma, myeloma; 4. AML, pre-B-ALL, T-ALL, CLL; 5. disease clusters; was used to
217 evaluate disease or subtype specific drug target expression. Statistical significance of binary
218 feature enrichment (e.g. high expression state) in a particular sample group was first
219 evaluated using the hypergeometric enrichment test, followed by Bonferroni adjustment of *P*-
220 values. If >90 % of the samples had high expression for a gene in the disease context, Inf
221 score was assigned instead of $-\log_{10}$ *P*-value (hypergeometric test would not be meaningful
222 if the sample size was close to the whole population). Each significant gene was uniquely
223 assigned to the disease group with the lowest *P*-value. In the case of equal *P*-values, a
224 broader disease category was prioritized using the disease hierarchy. As a second filtering
225 level, the Wilcoxon test was used to test whether the drug target gene is expressed at higher
226 level in cancer compared to normal erythroid, myeloid, B-lymphoid or T-lymphoid samples.
227 One normal sample group comparison was accepted for downstream analysis (with the
228 respective comparison annotated as failed). *In silico* drug analysis was benchmarked using
229 two case studies: drugs from Frismantas et. al. (33) and secondly known vulnerabilities (in
230 clinical use/trial). Success rate was reported for drug target gene expression in disease,
231 specificity for disease/subtypes and higher expression relative to normal cells.

232

233 **BeatAML drug analysis**

234

235 Spearman's correlation was computed for each drug area under curve (AUC) values and
236 cancer-map clusters, drug target genes or target gene mutations. Furthermore, mutations
237 with at least 5 observations and significant correlation adj. $P < 0.05$ to drug AUC values or
238 significant fisher exact test adj. $P < 0.05$ in cancer-map clusters were added as features that
239 could improve drug sensitivity prediction.

240

241 From total of 122 drugs 47 were excluded based on three criteria. First, 25 drugs with IC50
242 lower quartile below 10 nm were excluded as these drugs have limited efficacy. Second, 9
243 drugs with less than 80 samples with measured drug responses were excluded. Third, only
244 drugs with drug target information were kept, resulting in total of 75 drugs. The elastic net
245 implemented in glmnet (34) was trained using tenfold cross-validation using caret (35)
246 trainControl and repeatedcv method. Caret function train and its functionality tuneGrid was
247 used to optimize alpha parameter denoting the L1 and L2 regularization term proportions for
248 elastic net. Each drug had three categories of features to fit the model: clusters, drug target
249 gene expression, or mutations. To test the importance of each category in model fitting,

250 sample order was randomly shuffled for one category while the original order was preserved
251 for the other categories. Therefore, if the shuffled category features were important for the
252 model fit, model overall fit should decrease as the other features are unchanged. This
253 process was repeated 100 times and median of RMSE and R^2 values were computed. Only
254 drugs with good fit when using all the features were kept, having R^2 over 0.25 and RMSE
255 less than 0.9.

256

257 **Drug sensitivity testing using patient and healthy donor samples**

258 Bone marrow (BM) aspirates or peripheral blood samples were obtained from AML patients
259 ($N=52$) and healthy donors ($N=15$) after informed written consent using protocols approved
260 by a local Institutional Review Board and in accordance with the Declaration of Helsinki.
261 Mononuclear cells (MNCs) were isolated by density gradient separation (Ficoll-Paque
262 PREMIUM; GE Healthcare, Little Chalfont Bucks, UK) and immediately used for drug testing.
263 Cells were maintained in Mononuclear Cell Medium (MCM; Promocell) or in a 25% HS-5
264 conditioned medium plus 75% RPMI 1640 medium mix (CM). Palbociclib and idarubicin
265 (from Selleck, Houston, TX) were solvated in dimethyl sulfoxide and plated in 5 different
266 concentrations in 10-fold dilutions on 384-well plates using an Echo acoustic dispenser
267 (Labcyte, Sunnyvale, CA, USA), 1-10 000 nM for Palbociclib; 0.1-1000 nM for Idarubicin. 10
268 000 cells were added per well and incubated with the drugs for 3 days at 37°C, 5% CO₂.
269 Viability was measured using the CellTiter-Glo reagent (Promega, Madison, WI, USA)
270 according to the manufacturer's instructions and using the PHERAstar (BMG LABTECH,
271 Ortenberg, Germany) or SpectraMax Paradigm (Molecular Devices, Sunnyvale, CA, USA)
272 plate readers. Sensitivity to the drugs was quantified using a drug sensitivity score (DSS),
273 which is a modified area under the curve based metric described previously (36). A selective
274 DSS value was calculated by subtracting the mean DSS of the healthy BM controls from the
275 DSS of individual AML samples.

276

277 **Immunohistochemistry**

278 Anti-DPEP1 antibody (Atlas antibodies, rabbit polyclonal IgG against human renal
279 dipeptidase 1, product number: HPA009426, lot number: A57960) was used with the dilution
280 1:2500 to stain formalin fixed and paraffin embedded bone marrow trephine biopsy samples
281 from pediatric pre-B-ALL patients from the Pirkanmaa ERVA area between the years 2000
282 and 2017. 126 diagnostic samples (including also one Burkitt's lymphoma and a T-
283 lymphoblastic leukaemia/lymphoma case) were stained with a Ventana Benchmark GX
284 using UltraView Universal DAB Detection Kit. Cytoplasmic and membranous staining was
285 graded negative if less than 20 percent of the leukemic blasts were stained, positive if 20

286 percent or less than 50 percent of the blasts were positively stained and strong positive if 50
287 percent or a greater proportion of the blasts were positive. The analysis was performed by
288 two pathologists without the knowledge of the patient data or the interpretation of the other
289 analyst. The samples and clinical data were studied with the approval of the Tampere
290 University Hospital Ethical committee (#R16054 and #R13109) and in accordance with the
291 Declaration of Helsinki.

292

293 **Interactive web resource for data analysis**

294 The interactive online resource and the accompanying user guide for the Hemap resource
295 are described in more detail in the Methods Supplement and available at <http://hemap.uta.fi/>

296

297

297 **Results**

298

299 **Integrating transcriptomes to characterize molecular states across hematologic malignancies**

301 For the comparative analysis of hematologic malignancies on molecular level, we assembled
302 gene expression profiles from the NCBI GEO database (9), comprising patient samples
303 representing different cancers and proliferative disorders, and including cell lines and normal
304 blood cell types as controls. Sample annotations were curated, and each sample was
305 assigned a disease category. After data quality control and bias correction (see **Methods**,
306 **Fig. S1**), 9,544 samples comprise the final dataset (denoted “Hemap” samples) for
307 subsequent analysis, including 7,279 patient samples (mainly diagnostic) from hematologic
308 malignancies (**Fig. 1A, Tables S1 and S2**).

309

310 To enable discovery and statistical comparison of previously known and novel molecular
311 phenotypes alongside the annotated disease classes, we utilized a data-driven approach
312 that allows discovery of sample groups and visualizes these for interpretation. First, we
313 compared dimensionality reduction methods that allow visualization of complex data in two
314 dimensional space. The data representation accuracy was quantitatively assessed using the
315 metrics of continuity, trustworthiness and k-nearest neighbor (k-NN) classifier error (see
316 **Methods, Fig. S2**). As a result, t-Distributed Stochastic Neighbor Embedding (t-SNE) (18)
317 and its approximation, Barnes-Hut-SNE (BH-SNE) (19), was selected, as it performed
318 robustly (continuity and trustworthiness, 0.9860 and 0.9943, respectively) in two dimensions

319 and still preserved the neighborhood structure (k-NN error 0.0668) (**Figure S2**). The t-SNE
320 map was then utilized for density-based clustering to assign each sample to a cluster (**Fig.**
321 **1B**, see **Methods** for details) and the results were compared to annotated disease classes
322 (**Fig. 1C**). We conclude that both quantitative and biological assessments confirm that our
323 approach faithfully organizes the samples in an unsupervised manner based on their
324 molecular phenotype and disease type. We denote the resulting data-driven sample
325 grouping as the Hemap “cancer-map” in the following text.

326

327 **Comparative analysis associates clinical annotations and pathway activity to the** 328 **molecular disease stratification**

329 The 2D cancer-map revealed a clinically relevant sub-structure (**Table S2**), as exemplified
330 by the different B-cell lymphomas and pre-B-ALL cytogenetic subtypes (colored in **Figs. 2A**
331 **and B**, respectively), providing biological validation for separation of relevant phenotypes on
332 the cancer-map. A detailed comparison to annotations is presented in **Table S2**. Next,
333 statistically significant associations of clusters with gene expression levels, clinical
334 annotations and pathway enrichment scores across different databases were calculated (see
335 **Methods**). These results can be interactively tabulated and visualized using the online
336 Hemap resource. We selected five most significant pathways at disease cluster level, or
337 those matching pre-B-ALL subtype clusters (**Fig. 2C**) for visualization in a heatmap (see also
338 Table S5). In AML, the pathways for hematopoietic stem cell differentiation, pentose
339 phosphate pathway, renin-angiotensin system, IL-8/CXCR1-mediated signaling events and
340 C-MYB transcription factor networks were most significantly enriched. These reflect well the
341 known progenitor-like phenotype of AML cells. Pentose phosphate pathway, on the other
342 hand, represents a recently uncovered vulnerability (37,38) that is important for AML growth.
343 Similar disease-relevant pathways were also uncovered from T-ALL (TCR pathway), CLL
344 (BCR signaling pathway), lymphomas (cell adhesion molecules (39)) and multiple myeloma
345 (N-glycan biosynthesis (40,41)). In pre-B-ALL clusters, processes related to transcriptional
346 regulation were highly significant (including histone modification, CTCF pathway, and RNA
347 processing). WNT signaling (42,43) was found as a cluster 29-specific (t1;19) enriched
348 pathway, which matches its known relevance in these TCF3-PBX1 fusion carrying cases.
349 Samples expressing a gene or pathway of interest can be visualized as shown in **Fig. 2D**,
350 distinguishing the progenitor-like MLL subtype of pre-B-ALL based on the lack of expression
351 of the differentiation marker *MME* (also known as *CD10*) that is used in clinical diagnostics

352 (Fig. 2E). Similarly, most significant associations between disease clusters and drug
353 signatures can be examined by e-staining their significance (in red), as illustrated by
354 association of PI3K inhibitor BEZ235 gene set signature from DsigDB to pre-B-ALL (Fig.
355 2F), which validates a known association between a drug and a disease subtype. Further
356 analysis on the BEZ235 gene set and several case studies on how to generate novel
357 hypothesis are presented in the accompanying **User guide** to demonstrate different analysis
358 (refer to “Explore” and “e-staining” examples).

359

360 **Pan-cancer analysis to recognize vulnerabilities across disease contexts**

361 Parallel to molecular stratification, the diversity of patient profiles in Hemap has the potential
362 to support the development of new therapeutic strategies by leveraging the information
363 about the expression profiles across hematologic malignancies. We analyzed the specificity
364 of drug target expression states across patient groups in a hierarchical manner (**Methods**),
365 as illustrated in **Fig. 3A** (see also **Table S3** for a list of drugs and their targets and **Table S4**
366 for significant associations listed by disease hierarchy). The corresponding significance
367 ranking for targets of approved drugs is shown as heatmaps in **Fig. 3A-B**, where the
368 columns represent different disease contexts and gene targets (in rows) are sorted
369 according to their most significant association. The clinical indication for the drug(s) that
370 could be used to target each gene is indicated in the panel on the right, while e-staining
371 results for example drug targets are shown in **Fig. 3C** (see also **Fig. S3**). Proteasome
372 targeting drugs Bortezomib and Carfilzomib are in use for lymphomas and multiple myeloma.
373 Accordingly, 10/20 genes encoding the proteasome subunits are associated to this disease
374 hierarchy level, or to the pan-cancer category, with highest significance (**Fig. 3A**). In
375 comparison, for precision drugs such as the antibody drugs Elotuzumab (*SLAMF7*, P-val <
376 1e-315) or Daratumumab (*CD38*, P-val 1e-196) approved for MM, or Rituximab (*MS4A1*, P-
377 val < 1e-315 in LY+CLL) used in lymphomas and CLL (**Fig. 3A**) the specific gene targets
378 can be examined. Among all known vulnerabilities (drugs in clinical use / trial) a gene-level
379 analysis detected 84% of targets expressed and 69% were associated with highest
380 specificity score (-log₁₀ P-value) to the respective disease context (see **Table S3**). This is
381 exemplified by the comparison of genes with significant association to lymphoid leukemias
382 (**Fig. 3B**). *BCL2* targeted by venetoclax is shown as an example of an approved target in
383 CLL that our analysis associates with this disease context and with potential for targeting in
384 MM. The genes marked with asterisk, including *IL2RA* indicate targets of drugs approved for

385 other hematologic malignancies. Our analysis associated these with re-purposing potential in
386 CLL and/or ALL. *FLT3* is a recently approved target with disease cluster-specific expression
387 in B-lymphoid and myeloid leukemias.

388

389 **Utility of molecular disease stratification for evaluating drug screen results**

390 Next, we examined leukemias at disease subtype level from two *ex vivo* drug screening
391 datasets (12,33). Venetoclax had lower efficacy in T-ALL vs. B-ALL and lowest efficacy was
392 in t1;19 samples in the ALL drug screen (33) which agrees with Venetoclax target *BCL2*
393 gene expression in Hemap (**Fig. 3C**). Topotecan and dasatinib had the opposite profile, also
394 in agreement with subtype-specific expression of their targets *TOP1MT* and *LCK* (**Fig. S3**).
395 Taken together, out of 15 drugs from this ALL screen tested with our hierarchical analysis,
396 14 (93 %) had a candidate target expressed and 12 (80%) received highest target indication
397 in ALL (**Table S4**). Using the larger beatAML dataset (12), we set out to examine in an
398 unbiased manner what matters more in predicting drug responsiveness: target expression,
399 genetic lesions traditionally used to stratify patients, or the molecular phenotype as defined
400 by clustering of transcriptome states. We implemented models using elastic nets, where a
401 model for each drug (75 in total) was fit using these three categories of features. To test their
402 importance for model fitting, sample order was randomly shuffled for one category while the
403 original order was preserved for the other categories. The results for 11 drugs that achieved
404 the best overall model fit ($R^2 > 0.25$) are shown in **Fig. 4A**, including Venetoclax,
405 Panobinostat (HDAC inhibitor), Palbociclib (CDK4/6 inhibitor), 7 kinase inhibitors (many
406 targeting *FLT3*) and an ALK inhibitor. The average R^2 value from 100 tests is colored in the
407 heatmap and summarized as a boxplot next to it. If the shuffled feature was important for the
408 model fit, a decrease in R^2 is expected (shift from darker red to dimmer or blue colors) as the
409 other features are unchanged. For venetoclax, this analysis implicated target gene
410 expression as the main predictor (**Fig. S4**). For *FLT3*-targeting compounds, *FLT3* mutation
411 status was implicated as the top predictive feature (**Fig. S4**). However, overall, the lack of
412 cluster features in the model resulted in lowest predictive power. The disease clusters were
413 the best predictors for Palbociclib and Panobinostat, whereas mutation status had no effect
414 on their model fit. Panobinostat and Palbociclib showed opposite drug responses in clusters
415 13, 2, 6 compared to cluster 1 (**Fig. 4B**). Hemap clusters 17, 5, and 6 corresponded to these
416 clusters (**Fig. S4**) and were similarly enriched for *NPM1* and *FLT3* mutations or *PML-RARA*
417 fusion in both data sets. Comparison of clinical phenotypes revealed that blast morphology

418 was different between the clusters, linking maturation level to the differential drug response
419 (**Fig. 4C and Fig. S4**).

420

421 Classical targets involved in DNA metabolism (*TOP2A* and *B*) and clinically interesting
422 targets, including *CDK6*, *BCL2*, *MDM2* and *VEGFR2* from clinical trials, ranked highly in our
423 disease hierarchy analysis, as shown in **Figs. 3** and **S3**. However, when compared to
424 normal cell types, only 7% of the targets had higher expression in disease than in normal
425 cells (**Table S3**). Palbociclib target *CDK6* is highly expressed in all acute leukemias
426 compared to normal blood cell types, while *TOP2A* has high mRNA levels also in normal
427 blood cells (**Fig. 4D**). To evaluate drug sensitivity that is specific to cancer cells, an
428 experimental *ex vivo* screening approach is exemplified in **Fig. 4D** by comparing in AML
429 patient cell responses to the CDK4/6 inhibitor Palbociclib and Idarubicin targeting *TOP2A*
430 (see **Methods**). Drug sensitivity and selective drug sensitivity scores (DSS and sDSS,
431 respectively, see **Methods**) (36) are compared in box plots (**Fig. 4E**). Overall, the AML
432 patient bone marrow *ex vivo* cultures were more responsive to Idarubicin (refer to **Fig. S4** for
433 AML cell line data). However, a negative score indicating higher effect on normal bone
434 marrow cell viability was observed for Idarubicin in a larger fraction of AML cases compared
435 to Palbociclib. This observation of non-specific response, implied by negative sDSS score, is
436 consistent with our predictions from Hemap data. Therefore, the normal samples included in
437 Hemap could provide valuable additional information for drug target selection. Comparison
438 of *BCL2* and *BCL2L1* (also known as BCL-XL) levels are presented as another example in
439 **Fig. S4**, relevant to Venetoclax vs Navitoclax toxicity in targeting apoptosis. The Advanced
440 Use Case in the Hemap **User guide** extends this analysis using pathway activities and drug
441 chemical screen data.

442

443 **Evaluating new therapeutic strategies in a pan-hematologic cancer context**

444 Epigenetic regulation has emerged as an important mechanism that can corrupt the gene
445 regulatory network (44), motivating novel therapeutic approaches. Utilizing the disease
446 spectrum in Hemap, we performed a pan-hematologic cancer analysis of epigenetic
447 modifiers (**Table S5**), focusing on genes encoding proteins that are validated targets of small
448 molecule drugs (available from ChEMBL (28)). We found elevated expression of this set of
449 genes significantly enriched in CLL, T-ALL and clusters 28 (pre-B-ALL) and 32 (AML) (**Fig.**
450 **5A**, hypergeometric test adjusted *P*-values 0.0003, 0.0074, 0.0127, 0.0174, respectively, see

451 also **Table S5** for additional mutation frequency information (45) for the genes shown). The
452 expression state for six most significant genes from CLL are shown on the Hemap cancer-
453 map (**Fig. 5A**) and from independent validation RNA-seq data (46) (**Fig. 5B**).

454

455 A second promising new strategy, immunotherapy, can kill cancer cells by targeting surface
456 proteins with antibodies (47) or chimeric antigen receptors (48). However, side effects due to
457 targeting normal blood cells along with development of resistance occur (49). To provide a
458 rational basis for extending the target repertoire, we used disease hierarchy analysis to rank
459 996 candidates available in the Cell Surface Protein Atlas (32) (**Table S6**) resulting in broad,
460 disease and subtype-specific candidates. The top ranked candidate genes in our analysis
461 correspond to those that are uniformly high expressed within the specified disease context.
462 The stem cell antigen CD33, actively pursued for treatment of AML (50), is among highly
463 ranked surface targets in clinical trials shown in **Fig. S3**. Next, we obtained proteomics
464 profiles from 19 B-ALL patients (51) to compare our ranked list for pre-B-ALL (refer to **Table**
465 **S6**) to protein-level expression. The trend between *in silico* drug target rank and protein
466 detection rate is plotted in **Fig. 5C**. Validation rate for top candidates was above 75%. The
467 highly ranked surface targets *CLEC14A*, *DPEP1*, *CELSR2*, *MME*, *SDK2*, *INSR*, *GPM6B*,
468 *ELFN2*, *FLT3*, *SLC22A16*, *FLT4* and *APCDD1* correspond to those with higher expression in
469 pre-B-ALL patients compared to normal blood cells (see also **Fig. S5**). The high gene
470 expression state of *DPEP1* (**Fig. 5D**) in pre-B-ALL was further validated at protein level
471 based on immunohistochemistry of diagnostic bone marrow biopsies. The grading from 117
472 ALL bone marrows and 16 samples representing other lymphoid malignancies or normal
473 lymphoid tissues is presented in **Table 1** and illustrated in **Fig. 5E**.

474

475 To further facilitate the utilization of the data, pre-calculated results are accessible via our
476 interactive web resource (<http://hemap.uta.fi/>) including the expression state for 4,277 drug
477 target gene sets and 1,094 drug response signatures, which can be further investigated in
478 the context of the 12,433 pathways and molecular signatures (see **Methods** and **User guide**
479 examples). Disease hierarchy analysis for the curated list of drug to target gene associations
480 (11,373 drugs; 1,182 genes) from the Therapeutic Target Database (TTD) (29), DGIdb (30)
481 and targets of FDA approved drugs across disease (31) is available in **Table S4**. In this
482 manner, *in silico* drug target selection based on Hemap can leverage gene and pathway
483 expression, as evaluated across cancer types and normal blood cell types.

484

485

Discussion

486

487 The integration of available genome-wide data from patients allows uncovering shared
488 disease mechanisms and new therapeutic options. Recent work has highlighted that
489 molecular and genetic data that helps stratify patients can dramatically increase the
490 likelihood of success during clinical development (8,52). However, in several cancer types,
491 including those of hematopoietic and lymphoid tissues, the majority of data have been
492 collected by separate studies concentrating on certain cancer types, which hinders the
493 identification of cancer type specific features. We present an interactive online resource,
494 Hemap (<http://hemap.uta.fi/>) for analysis across multi-center gene expression datasets to
495 investigate disease subgroups and compare molecular phenotypes across 9,544 samples
496 from hematologic malignancies.

497

498 In practice, the samples included to Hemap are inaccessible to most clinical researchers.
499 The Hemap resource serves to re-purpose data from public repositories for clinical
500 interpretation in an intuitive manner that does not require data analysis expertise. In future
501 versions of Hemap, we plan to include also RNA-seq studies. Presently, the resource
502 already contains the TCGA AML dataset and the User Guide includes examples using this
503 data. Alongside curated disease assignment, we present a data-driven approach that
504 organizes and integrates heterogeneous sample collections in an unbiased manner. To
505 facilitate this, we demonstrated how unsupervised clustering and dimensionality reduction
506 methods, here by the t-SNE method, can be used for organizing the molecular profiles for
507 further downstream analysis. The high level of performance of t-SNE has been shown in
508 context of various data types (18,53-54). In this manner, genes characterizing the patient
509 clusters can be identified for further delineation of their functional role. In CLL, our analysis
510 implicates high expression of several polycomb group proteins (SFMBT1, CBX7 and EZH1)
511 in CLL that could be targeted by small molecules, in line with chromatin state data (46), and
512 their mutation (45) frequencies, highlighting the importance to consider the spectrum of
513 genetic and epigenetic changes in these malignancies. Earlier studies have implicated
514 epigenetic plasticity as a key driver of CLL evolution during treatment (55). Specifically, CLL
515 cases had little to no genetic subclonal evolution, while significant recurrent DNA methylation
516 changes were enriched for regions near Polycomb targets (55). To further elucidate the

517 mechanisms, inclusion of post-treatment data and integrating methylation, chromatin marker
518 and mutation profiles represent important future directions in developing the Hemap
519 resource.

520

521 From a therapeutic perspective, approaches for the development of treatment strategies with
522 a broad disease focus and molecular subtype resolution are urgently needed. We used
523 Hemap to provide a roadmap for candidate drug therapies that allows prioritizing new
524 candidates based on disease-specificity. Our analysis recapitulated known vulnerabilities,
525 providing additional confirmation for targets in current clinical trials: Several compounds
526 targeting Bcl2 have been developed and have shown promise in treating both CLL and Non-
527 Hodgkin's lymphoma (56-57). However, navitoclax that also targets *BCL2L1* (also known as
528 BCL-XL) displays platelet toxicity. This potential for off-target effects was visible as high
529 gene expression level in the erythroid lineage, supporting the choice of the more selective
530 venetoclax. The prevalent high expression also in MM and pre-B-ALL found in our study
531 provides a rationale for the expansion of the testing of these compounds in lymphoid
532 malignancies. This suggestion is additionally supported by a recent study showing that these
533 compounds have promise in MLL-rearranged ALL (58), a pre-B-ALL subtype corresponding
534 to cluster 29 in our dataset. However, Hemap analysis predicts insensitivity in T-ALL and
535 t1;19 subtype, matching recent ALL drug screen data (33). Similarly, the elevated expression
536 of the p53-regulating MDM2 in pre-B-ALL fits with recent data on successful application of
537 antagonists in clinical trials (59), and mechanisms for its high expression ETV6-RUNX1-
538 positive leukemias (60).

539

540 Presently no drug screens have been carried out in primary patient cells across the
541 spectrum of hematologic malignancies in Hemap. The utility of Hemap for drug repurposing
542 was demonstrated in our recent study that identified dasatinib as a targeted therapy for a
543 subgroup of T-ALL patients (61). Here, we examined drug screen datasets to examine how
544 differential drug responsiveness could be linked to disease sub-clusters and drug targets
545 identified from the cancer maps. Using the beatAML dataset, we systematically compared
546 the importance of mutations, clusters and drug target gene expression in predicting drug
547 responses. Clusters were the best predictors of drug response for drugs with best overall
548 model fit. However, the importance of each predictor was largely influenced by drug type.
549 Best predictor for Venetoclax response was *BCL2* expression level. *FLT3* mutation status

550 and other mutations were the best predictors for kinase inhibitors. In contrast, disease
551 clusters were the best predictors for Palbociclib and Panobinostat responses to which
552 mutation status had no effect on model fit. Comparison of clusters in which Panobinostat and
553 Palbociclib showed opposite drug responses revealed that blast morphology was different,
554 linking maturation level to differential drug response. Furthermore, their drug targets were
555 differentially expressed in these clusters, pointing out the importance of integrating context
556 and drug target expression for *in-silico* drug screening. Surprisingly, the HDAC expression
557 pattern revealed cytosolic members (*HDAC6* and *HDAC10* (62)) as resistance markers,
558 while nuclear *HDAC4* and *HDAC9* correlated with sensitivity. Our analysis also supported
559 *CDK4/6* as disease specific targets that are known to act as critical activators of normal and
560 leukemic HSC (63). Here, Palbociclib compared favorably to Idarubicin regarding patient
561 blast sensitivity against normal bone marrow cells, reflected in mRNA data from Hemap. The
562 selectivity over normal cells may improve further using combination therapy (63) that allows
563 decreasing the dose. However, additional parameters such as drug target protein level, drug
564 metabolism and cell proliferation rate further contribute to sensitivity and therefore not all
565 patients matching a molecular subtype or expressing the target mRNA can be expected to
566 respond favorably.

567

568 Cancer cells display remarkable plasticity: resistance to recently approved CD19-targeting
569 CAR-T therapy has been shown to occur via mutations or splicing defects at the CD19 locus
570 or lineage-switching (49). To combat the diversity of resistance mechanisms, there is a
571 demand to diversify the target repertoire. In pre-B-ALL, we identified promising surface
572 protein candidates, prioritizing targets with consistently high levels within the given disease
573 context and low levels in normal blood cell types. Over 75% of the highly ranked candidates
574 were confirmed using proteomics (51), and additional literature confirmation was found for
575 five candidates. Moreover, we validated DPEP1 as a potential surface target in pre-B-ALL by
576 immunohistochemical staining of diagnostic bone marrow biopsies. Positive staining was
577 found in each subtype for majority of cases, except in MLL where both the Hemap gene
578 expression data and protein staining indicated low or undetectable levels. The validation
579 cohort consisted of pediatric cases, while Hemap analysis included also adult samples.
580 DPEP1 is a zinc-dependent metalloproteinase that is expressed aberrantly in several
581 cancers, and has been implicated as a potential therapeutic target in colon and pancreatic

582 cancers (64,65). In future, increased availability of protein-level data from different
583 hematologic malignancies will allow confirming additional targets.

584

585 In conclusion, the interactive Hemap resource facilitates comparative analyses across
586 multiple hematologic malignancies. We envision that the mechanistic insight gained by
587 concomitant identification of molecular subtypes, genetic aberrations and derailed cellular
588 pathways will expedite therapeutic innovations and clinical utility.

589

590

591

Acknowledgements

592 We would like to thank the Finnish Pharmaceutical Information Centre Ltd for information
593 provided regarding approved drugs in hematologic malignancies, Dr. Aik Choon Tan for the
594 advice with drug signature gene sets, staff of the FIMM Technology Center High-Throughput
595 Biomedicine Unit and Sequencing Lab. Members of the T. Aittokallio, C.A. Heckman, O.
596 Kallioniemi, S. Mustjoki, K. Porkka and K. Wennerberg groups for their help to analyze drug
597 response profiles, and Dr. Sheila Reynolds and Roger Kramer for assistance with feature
598 matrix analysis. The work was supported by grants from the Academy of Finland (project no.
599 312043 (MN), no. 310829 (MN), no. 259038 (KG), no. 276634 (MH), no. 277816 (OL)), The
600 Finnish Cultural Foundation (Interdisciplinary Science Workshops, MH), Sigrid Juselius
601 Foundation (MN), and Cancer Society of Finland (MN, MH, OL, KG), Paulo Foundation (OL),
602 Foundation for Pediatric Research (OL), Jane and Aatos Erkko Foundation (OL), Nokia
603 Foundation (VH) and University of Eastern Finland (MH). We thank CSC – IT Center for
604 Science and UEF bioinformatics center for providing computational resources.

605

606

607

References

608

609

610

611

612

613

614

615

616

1. Orr MS, Scherf U. Large-scale gene expression analysis in molecular target discovery. *Leukemia*. **2002**;16:473–7.
2. Ylipää A, Yli-Harja O, Zhang W, Nykter M. Characterization of aberrant pathways across human cancers. *BMC Syst. Biol.* **2013**;7:S1.
3. Kumar SK, Rajkumar V, Kyle RA, van Duin M, Sonneveld P, Mateos MV, *et al.* Multiple myeloma. *Nat Rev Dis Primers*. **2017**;3:17046.
4. Nangalia J, Green AR. Myeloproliferative neoplasms: from origins to outcomes. *Blood*. **2017**;130:2475-83.

- 617 5. June CH, O'Connor RS, Kawalekar OU, Ghassemi S, Milone MC. CAR T cell
618 immunotherapy for human cancer. *Science*. **2018**;359:1361-65.
- 619 6. McCabe B, Liberante F, Mills KI. Repurposing medicinal compounds for blood cancer
620 treatment. *Ann. Hematol.* **2015**;94:1267–76.
- 621 7. Corces-Zimmerman MR, Hong WJ, Weissman IL, Medeiros BC, Majeti R.
622 Preleukemic mutations in human acute myeloid leukemia affect epigenetic regulators
623 and persist in remission. *Proc. Natl. Acad. Sci. U. S. A.* **2014**;111:2548–53.
- 624 8. Iorio F, Knijnenburg TA, Vis DJ, Bignell GR, Menden MP, Schubert M, *et al.* A
625 Landscape of Pharmacogenomic Interactions in Cancer. *Cell*. **2016**;166:740-54.
- 626 9. Edgar R, Domrachev M, Lash AE. Gene Expression Omnibus: NCBI gene expression
627 and hybridization array data repository. *Nucleic Acids Res.* **2002**;30:207-10.
- 628 10. Irizarry RA, Bolstad BM, Collin F, Cope LM, Hobbs B, Speed TP. Summaries of
629 Affymetrix GeneChip probe level data. *Nucleic Acids Res.* **2003**;31:e15.
- 630 11. Eklund AC, Szallasi Z. Correction of technical bias in clinical microarray data
631 improves concordance with known biological information. *Genome Biol.* **2008**;9:R26.
- 632 12. Tyner JW, Tognon CE, Bottomly D, Wilmot B, Kurtz SE, Savage SL, *et al.* Functional
633 genomic landscape of acute myeloid leukaemia. *Nature*. **2018**;562:526-31.
- 634 13. Lawrence ND. Gaussian process latent variable models for visualization of high
635 dimensional data. *Adv. Neural Inf. Process. Syst.* **2004**;16.3:329-36.
- 636 14. Roweis ST, Lawrence KS. Nonlinear dimensionality reduction by locally linear
637 embedding. *Science*. **2000**;290:2323-6.
- 638 15. Hotelling H. Analysis of a complex of statistical variables into principal components. *J.*
639 *Educ. Psychol.* **1933**;24:417.
- 640 16. Tipping ME, Bishop CM. Probabilistic Principal Component Analysis. *J. Roy. Stat.*
641 *Soc. B.* **1999**;61:611-22.
- 642 17. Sammon JW. A nonlinear mapping for data structure analysis. *IEEE T. Comput.*
643 **1969**;5:401-9.
- 644 18. van der Maaten L, Hinton G. Visualizing Data Using t-SNE. *J. Mach. Learn. Res.*
645 **2008**;9:2579–2605.
- 646 19. van der Maaten L. Accelerating t-SNE using Tree-Based Algorithms. *J. Mach. Learn*
647 *Res.* **2014**;15:1-21.
- 648 20. Mehtonen J, Pölönen P, Häyrynen S, Lin J, Liuksiala T, Granberg K, *et al.* Data-driven
649 characterization of molecular phenotypes across heterogenous sample collections.
650 *bioRxiv*. **2018**. <https://doi.org/10.1101/248096>.
- 651 21. Cancer Genome Atlas Research Network. Comprehensive molecular characterization
652 of gastric adenocarcinoma. *Nature*. **2014**;513:202-9.
- 653 22. Subramanian A, Tamayo P, Mootha VK, Mukherjee S, Ebert BL, Gillette MA, *et al.*
654 Gene set enrichment analysis: A knowledge-based approach for interpreting genome-
655 wide expression profiles. *Proc. Natl. Acad. Sci. U. S. A.* **2005**;102:15545-50.

- 656 23. Kutmon M, Riutta A, Nunes N, Hanspers K, Willighagen EL, Bohler A, *et al.*
657 WikiPathways: capturing the full diversity of pathway knowledge. *Nucleic Acids Res.*
658 **2015**;44:488-94.
- 659 24. Duarte NC, Becker SA, Jamshidi N, Thiele I, Mo ML, Vo TD, *et al.* Global
660 reconstruction of the human metabolic network based on genomic and bibliomic data.
661 *Proc. Natl. Acad. Sci. U. S. A.* **2007**;104:1777-82.
- 662 25. Cerami EG, Gross BE, Demir E, Rodchenkov I, Babur O, Anwar N, *et al.* Pathway
663 Commons, a web resource for biological pathway data. *Nucleic Acids Res.*
664 **2011**;39:685-90.
- 665 26. Yoo M, Shin J, Kim J, Ryall KA, Lee K, Lee S, *et al.* DSigDB: drug signatures
666 database for gene set analysis. *Bioinformatics.* **2015**;31:3069-71.
- 667 27. Hänzelmann S, Castelo R, Guinney J. GSVA: gene set variation analysis for
668 microarray and RNA-Seq data. *BMC Bioinformatics.* **2013**;14:7.
- 669 28. Bento AP, Gaulton A, Hersey A, Bellis LJ, Chambers J, Davies M, *et al.* The ChEMBL
670 bioactivity database: an update. *Nucleic Acids Res.* **2014**;42:D1083–90.
- 671 29. Yang H, Qin C, Li YH, Tao L, Zhou J, Yu CY, *et al.* Therapeutic target database
672 update 2016: enriched resource for bench to clinical drug target and targeted pathway
673 information. *Nucleic Acids Res.* **2016**;44:D1069-74.
- 674 30. Cotto KC, Wagner AH, Feng YY, Kiwala S, Coffman AC, Spies G, *et al.* DGIdb 3.0: a
675 redesign and expansion of the drug–gene interaction database. *Nucl Acids Res.*
676 **2018**;46:D1068–73.
- 677 31. Santos R, Ursu O, Gaulton A, Bento AP, Donadi RS, Bologa CG, *et al.* A
678 comprehensive map of molecular drug targets. *Nature Rev Drug Discov.* **2017**;16:19-
679 34.
- 680 32. Bausch-Fluck D, Hofmann A, Bock T, Frei AP, Cerciello F, Jacobs A, *et al.* A mass
681 spectrometric-derived cell surface protein atlas. *PLoS One.* **2015**;10:e0121314.
- 682 33. Frismantas V, Dobay MP, Rinaldi A, Tchinda J, Dunn SH, Kunz J, *et al.* Ex vivo drug
683 response profiling detects recurrent sensitivity patterns in drug-resistant acute
684 lymphoblastic leukemia. *Blood.* **2017**;129:e26-37.
- 685 34. Friedman J, Hastie T, Tibshirani R. Regularization Paths for Generalized Linear
686 Models via Coordinate Descent. *Journal of statistical software.* **2010**;33:1-22.
- 687 35. Kuhn M. Building predictive models in R using the caret package. *Journal of statistical*
688 *software.* **2008**;28:1-26.
- 689 36. Yadav B, Pemovska T, Szwajda A, Kuleskiy E, Kontro M, Karjalainen R, *et al.*
690 Quantitative scoring of differential drug sensitivity for individually optimized anticancer
691 therapies. *Sci. Rep.* **2014**;4:5193.
- 692 37. Bhanot H, Weisberg EL, Reddy MM, Nonami A, Neuberg D, Stone RM, *et al.* Acute
693 myeloid leukemia cells require 6-phosphogluconate dehydrogenase for cell growth
694 and NADPH-dependent metabolic reprogramming. *Oncotarget.* **2017**;8:67639-50.

- 695 38. Mizuno H, Kagoya Y, Koya J, Masamoto Y, Kurokawa M. Activated Pentose
696 Phosphate Pathway Mediated By Fbp-1 Upregulation Supports Progression of Acute
697 Myeloid Leukemia with High EVI-1 Expression. *Blood*. **2018**;132:757.
- 698 39. Drillenbug P, Pals ST. Cell adhesion receptors in lymphoma dissemination. *Blood*.
699 **2000**;95:1900-10.
- 700 40. Mittermayr S, Lê GN, Clarke C, Millán Martín S, Larkin, AM, O’Gorman P, *et al*.
701 Polyclonal immunoglobulin GN-glycosylation in the pathogenesis of plasma cell
702 disorders. *Journal of proteome research*. **2016**;16:748-62.
- 703 41. Pang X, Li H, Guan F, Li X. Multiple Roles of Glycans in Hematological Malignancies.
704 *Frontiers in oncology*. **2018**;8:364.
- 705 42. Diakos C, Xiao Y, Zheng S, Kager L, Dworzak M, Wiemels JL. Direct and indirect
706 targets of the E2A-PBX1 leukemia-specific fusion protein. *PloS one*. **2014**;9:e87602.
- 707 43. Karvonen H, Perttilä R, Niininen W, Hautanen V, Barker H, Murumägi A, *et al*. Wnt5a
708 and ROR1 activate non-canonical Wnt signaling via RhoA in TCF3-PBX1 acute
709 lymphoblastic leukemia and highlight new treatment strategies via Bcl-2 co-targeting.
710 *Oncogene*. **2019**;DOI:10.1038/s41388-018-0670-9.
- 711 44. Huether R, Dong L, Chen X, Wu G, Parker M, Wei L, *et al*. The landscape of somatic
712 mutations in epigenetic regulators across 1,000 paediatric cancer genomes. *Nat*
713 *Commun*. **2014**;5:3630.
- 714 45. Ramsay AJ, Martínez-Trillos A, Jares P, Rodríguez D, Kwarciak A, Quesada V. Next-
715 generation sequencing reveals the secrets of the chronic lymphocytic leukemia
716 genome. *Clin Transl Oncol*. **2013**;15:3-8.
- 717 46. Rendeiro AF, Schmidl C, Strefford JC, Walewska R, Davis Z, Farlik M, *et al*.
718 Chromatin accessibility maps of chronic lymphocytic leukaemia identify subtype-
719 specific epigenome signatures and transcription regulatory networks. *Nat Commun*.
720 **2016**;7:11938.
- 721 47. Robak T, Blonski JZ, Robak P. Antibody therapy alone and in combination with
722 targeted drugs in chronic lymphocytic leukemia. *Semin Oncol*. **2016**;43:280-90.
- 723 48. Maude SL, Frey N, Shaw PA, Aplenc R, Barrett DM, Bunin NJ, *et al*. Chimeric Antigen
724 Receptor T Cells for Sustained Remissions in Leukemia. *N. Engl. J. Med*.
725 **2014**;371:1507–17.
- 726 49. Jacoby E, Nguyen SM, Fountaine TJ, Welp K, Gryder B, Qin H, *et al*. CD19 CAR
727 immune pressure induces B-precursor acute lymphoblastic leukaemia lineage switch
728 exposing inherent leukaemic plasticity. *Nat Commun*. **2016**;7:12320.
- 729 50. Laszlo GS, Estey EH, Walter RB. The past and future of CD33 as therapeutic target in
730 acute myeloid leukemia. *Blood Rev*. **2014**;28:143–53.
- 731 51. Mirkowska P, Hofmann A, Sedek L, Slamova L, Mejstrikova E, Szczepanski T, *et al*.
732 Leukemia surfaceome analysis reveals new disease-associated features. *Blood*.
733 **2013**;121:e149-59.
- 734 52. Nelson MR, Tipney H, Painter JL, Shen J, Nicoletti P, Shen Y, *et al*. The support of
735 human genetic evidence for approved drug indications. *Nat genet*. **2015**;47:856-60.

- 736 53. Amir el-AD, Davis KL, Tadmor MD, Simonds EF, Levine JH, Bendall SC, *et al.* viSNE
737 enables visualization of high dimensional single-cell data and reveals phenotypic
738 heterogeneity of leukemia. *Nat Biotechnol.* **2013**;31:545-52.
- 739 54. Shekhar K, Brodin P, Davis MM, Chakraborty AK. Automatic Classification of Cellular
740 Expression by Nonlinear Stochastic Embedding (ACCENSE). *Proc. Natl. Acad. Sci.*
741 *U. S. A.* **2014**;111:202-7.
- 742 55. Smith EN, Ghia EM, DeBoever CM, Rassenti LZ, Jepsen K, Yoon KA, *et al.* Genetic
743 and epigenetic profiling of CLL disease progression reveals limited somatic evolution
744 and suggests a relationship to memory-cell development. *Blood Cancer J.*
745 **2015**;5:e303.
- 746 56. Anderson MA, Huang D, Roberts A. Targeting BCL2 for the treatment of lymphoid
747 malignancies. *Semin. Hematol.* **2014**;51:219–27.
- 748 57. Roberts AW, Davids MS, Pagel JM, Kahl BS, Puvvada SD, Gerecitano JF, *et al.*
749 Targeting BCL2 with Venetoclax in Relapsed Chronic Lymphocytic Leukemia. 2015.
750 *N. Engl. J. Med.* **2015**;374:311-22.
- 751 58. Benito JM, Godfrey L, Kojima K, Hogdal L, Wunderlich M, Geng H, *et al.* MLL-
752 Rearranged Acute Lymphoblastic Leukemias Activate BCL-2 through H3K79
753 Methylation and Are Sensitive to the BCL-2-Specific Antagonist ABT-199. *Cell Rep.*
754 **2015**;13:2715-27.
- 755 59. Andreeff M, Kelly KR, Yee K, Assouline S, Strair R, Popplewell L, *et al.* Results of the
756 Phase I Trial of RG7112, a Small-Molecule MDM2 Antagonist in Leukemia. *Clin.*
757 *Cancer Res.* **2015**;22:868-76.
- 758 60. Kaindl U, Morak M, Portsmouth C, Mecklenbräuker A, Kauer M, Zeginigg M, *et al.*
759 Blocking ETV6/RUNX1-induced MDM2 overexpression by Nutlin-3 reactivates p53
760 signaling in childhood leukemia. *Leukemia.* **2014**;28:600–8.
- 761 61. Laukkanen S, Grönroos T, Pölönen P, Kuusanmäki H, Mehtonen J, Cloos J, *et al.* *In*
762 *silico* and preclinical drug screening identifies dasatinib as a targeted therapy for T-
763 ALL. *Blood Cancer J.* **2017**;7:e604.
- 764 62. Boyault C, Sadoul K, Pabion M, Khochbin S. HDAC6, at the crossroads between
765 cytoskeleton and cell signaling by acetylation and ubiquitination. *Oncogene.* **2007**;26:
766 5468-76.
- 767 63. Yang C, Boyson CA, Di Liberto M, Huang X, Hannah J, Dorn DC, *et al.* CDK4/6
768 Inhibitor PD 0332991 Sensitizes Acute Myeloid Leukemia to Cytarabine-Mediated
769 Cytotoxicity. *Cancer Res.* **2015**;75:1838–45.
- 770 64. Zhang G, Schetter A, He P, Funamizu N, Gaedcke J, Ghadimi BM, *et al.* DPEP1
771 inhibits tumor cell invasiveness, enhances chemosensitivity and predicts clinical
772 outcome in pancreatic ductal adenocarcinoma. *PLoS one.* **2012**;7:e31507.
- 773 65. Eisenach PA, Soeth E, Röder C, Klöppel G, Tepel J, Kalthoff H, *et al.* Dipeptidase 1
774 (DPEP1) is a marker for the transition from low-grade to high-grade intraepithelial
775 neoplasia and an adverse prognostic factor in colorectal cancer. *British journal of*
776 *cancer.* **2013**;109:694-703.
- 777

778

779

Tables

780

781 **Table 1. DPEP1 protein expression in bone marrow biopsies based on**
 782 **immunohistochemistry grading.**

783

	DPEP1 Immunohistochemistry			Total
	Negative	Positive	Strong positive	
pre-B-ALL				
BCR-ABL1	0	2	0	2
ETV6-RUNX1	7	16	10	33
Hyperdiploid	13	16	1	30
Hypodiploid	1	0	0	1
MLL rearranged	5	0	0	5
TCF3-PBX1	4	0	0	4
other	18	16	8	42
Total	48	50	19	117
Other disease/tissues				
BL	2	0	0	2
T-lymphoblastic leukaemia/lymphoma	6	1	0	7

MCL	1	0	0	1
CLL	1	0	0	1
PTCL	1	0	0	1
CHL (NSCHL)	1	0	0	1
Tonsils	1	0	0	1
Thymus	1	0	0	1
Spleen	1	0	0	1
Total	15	1	0	16

784

785

786

787

Figures and Legends

788

789 **Figure 1. A molecular stratification of hematologic malignancies and normal blood**

790 **cell types is captured in a t-SNE visualization. A.** Composition of the hematologic

791 transcriptome dataset. Of the 9,544 samples, 6,820 represent hematologic malignancies

792 (leukemia, lymphoma or myeloma), and the rest consist of cancer cell lines, proliferative

793 diseases (myeloid denoted pM and lymphoid denoted pL), normal blood cells (healthy donor

794 or patient). See also **Table S2. B.** The transcriptome data projected in 2D using t-SNE is

795 shown. Each dot represents one of the 9,544 samples. Cluster assignment based on density

796 estimation is shown in color for seven distinct clusters visible on the cancer map. **C.** The

797 separation between annotated disease types (indicated by color) is shown: the lymphoid

798 malignancies separate into acute lymphoid leukemias (pre-B-ALL in pink and T-ALL in blue),

799 lymphomas (top right), multiple myeloma (adjacent to B-cell lymphomas) and chronic

800 lymphoblastic leukemia (CLL, below). The myeloid diseases (AML, CML and

801 myeloproliferative disease) are grouped closely. Samples representing normal cell types or

802 cell lines are in grey color. Numbers refer to data driven cluster assignment (see Table S2).

803

804

805 **Figure 2. Comparison of molecular phenotypes based on the cancer-map.** Sample

806 attribute visualizations are exemplified that allow characterizing the molecular phenotypes.

807 Different BCL types (in **A**) and pre-B-ALL subtypes (in **B**) are colored based on sample

808 annotations (refer to **Table S2** for abbreviations). **C.** The five most significant pathways per

809 disease cluster (above) or pre-B-ALL cluster (below) are shown as a heatmap (tones of red

810 indicate significant enrichment to cluster (hypergeometric test, scaled P-value). The pre-B-

811 ALL cluster number and color (as in B) are indicated below the heatmap. **D.** The bimodal

812 log₂ gene expression signal distribution can be used to separate samples with low or non-

813 detectable expression (N.D., in blue) from samples expressing the gene (in red).

814 Alternatively significance of enrichment for gene sets and pathways from different databases

815 can be selected for visualization (e-staining) on the cancer map. **E.** The corresponding gene

816 expression state is shown on the cancer-map for the B-lymphoid differentiation marker *MME*,

817 where the color tones correspond to scaled log₂ expression values (red: high, white low;

818 blue: not detected). **F.** Gene set enrichment for BEZ235 targets is e-stained, with empirical

819 P-value < 0.05 shown in red.

820

821 **Figure 3. Pan-cancer analysis associates disease contexts with therapeutic strategies.**

822 **A.** The *in silico* drug target analysis across disease hierarchy groups is illustrated
823 schematically and using proteasome and surface protein targeting drugs as examples. On
824 the left, the heatmap columns are organized by disease, and drug targets (in rows) are
825 sorted based on their most significant disease context association (red color tones indicate
826 significant P-value in hypergeometric test, $-\log(P)$). The adjacent heatmap shows the
827 disease indications for drugs known to target the gene in question. Notice that majority of
828 drugs target multiple genes, as illustrated by Bortezomib/Carfilzomib, and only some
829 correspond to precision drugs as exemplified by antibody targets (*SLAMF7*, *CD19*, *MS4A1*
830 and *CD38*). **B.** Comparison of targets of approved drugs with significant association to
831 lymphoid leukemias are shown as in **A**. The disease indications in dimmer red tone reveal
832 potential for re-purposing of drugs approved or in clinical trials in other disease indications
833 (notice that LE includes ALL and CLL). **C.** Example genes highlighted in the heatmaps are e-
834 stained on the t-SNE map as in **Fig. 2C**.

835

836

837 **Figure 4. Evaluation of cluster and disease specificity of drug responses. A.** A

838 heatmap comparing how well the drug response data fits different elastic net regression
839 models is shown (color indicates R^2 values, drugs with $R^2 > 0.25$ are shown). The values are
840 summarized as boxplot on the right. Full model included clusters (Clust), gene expression
841 (Gexp) and mutations (Mut), while one category is omitted in the other models. **B.**
842 Palbociclib and Panobinostat drug response AUC values are shown as boxplots for all AML
843 cases and for clusters correlated to differential drug response identified for Palbociclib and
844 Panobinostat. High AUC values mean drug resistance and low drug sensitivity. **C.** Heatmap
845 of FAB morphology markers, cluster specific genetic aberrations and drug target genes
846 (*CDK6* for Palbociclib and *HDAC4,6,10,2* for Panobinostat) are shown for same clusters as
847 in **B**. **D.** The gene expression data for *TOP2A* and *CDK6* are e-stained on cancermap.
848 Comparison to normal blood cell types is shown as boxplots of the log₂ gene expression
849 signal (T: T-lymphoid, B: B-lymphoid, E: erythroid and M: myeloid). For *CDK6* clusters
850 corresponding to beatAML clusters (as in **C**) are shown **E.** Drug sensitivity in an AML patient
851 cohort based on DSS and sDSS scores ($N = 52$) are shown as boxplots for Palbociclib
852 (*CDK4/6* inhibitor) and the approved AML drug (idarubicin). High difference between DSS

853 and sDSS values indicate response in the bone marrow normal mononuclear cells, whereas
854 low difference indicate selectivity in AML cells.

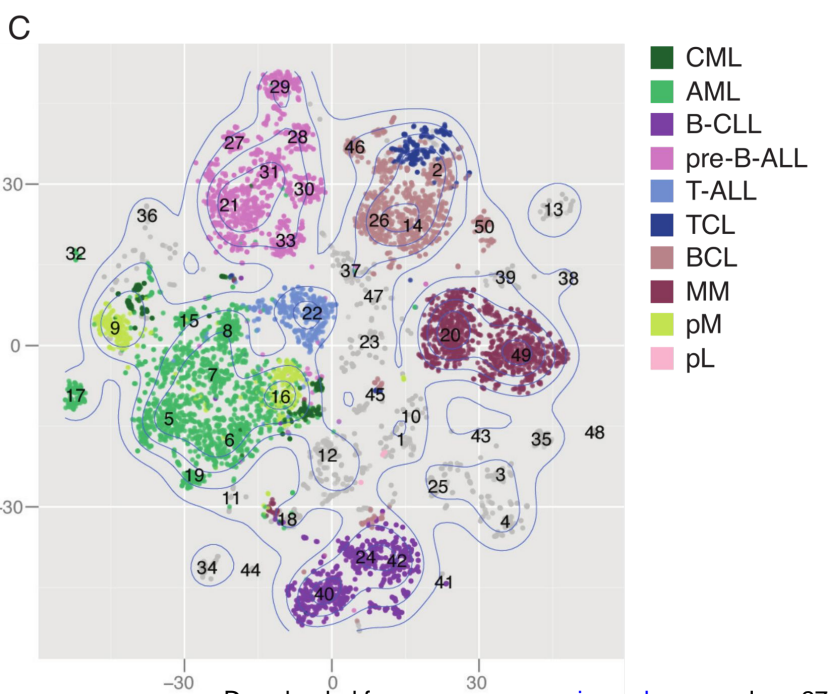
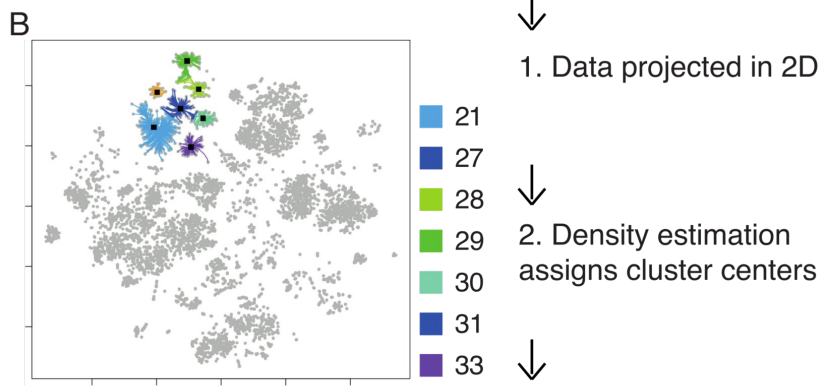
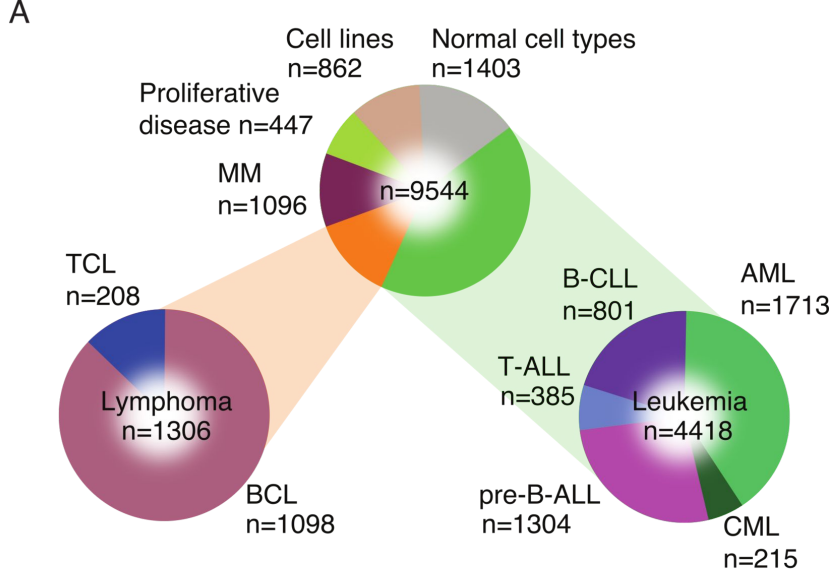
855

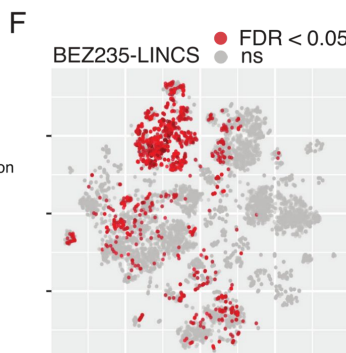
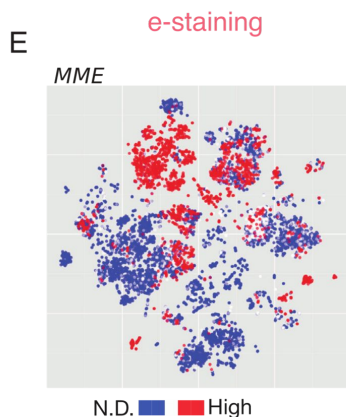
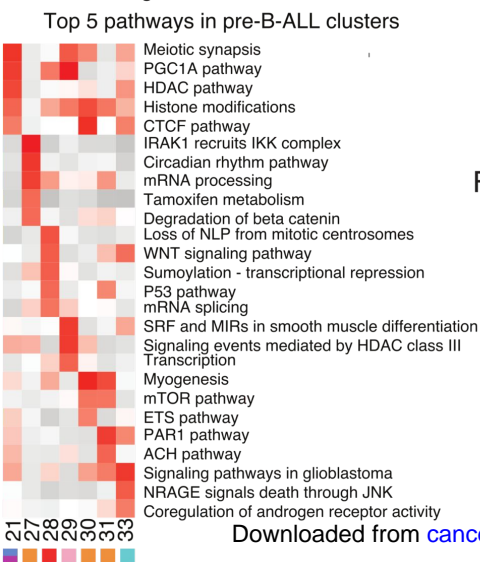
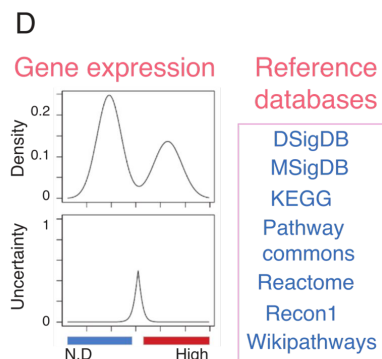
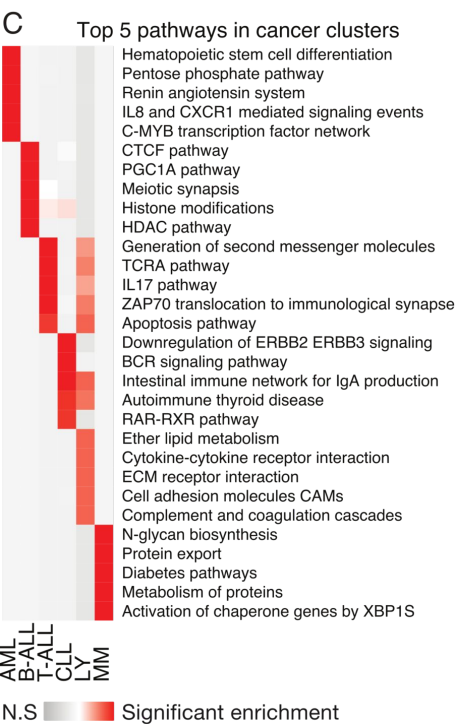
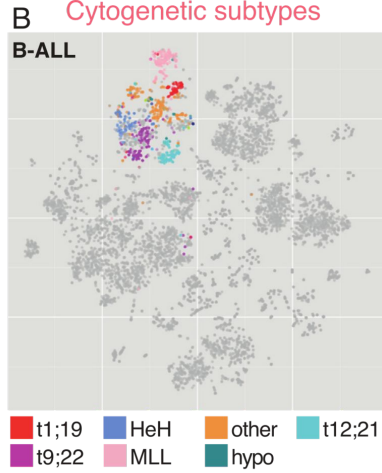
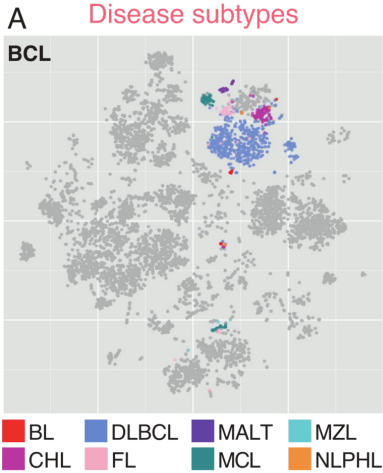
856 **Figure 5. Connecting the map of patient gene expression states to drug target**
857 **profiles. A.**

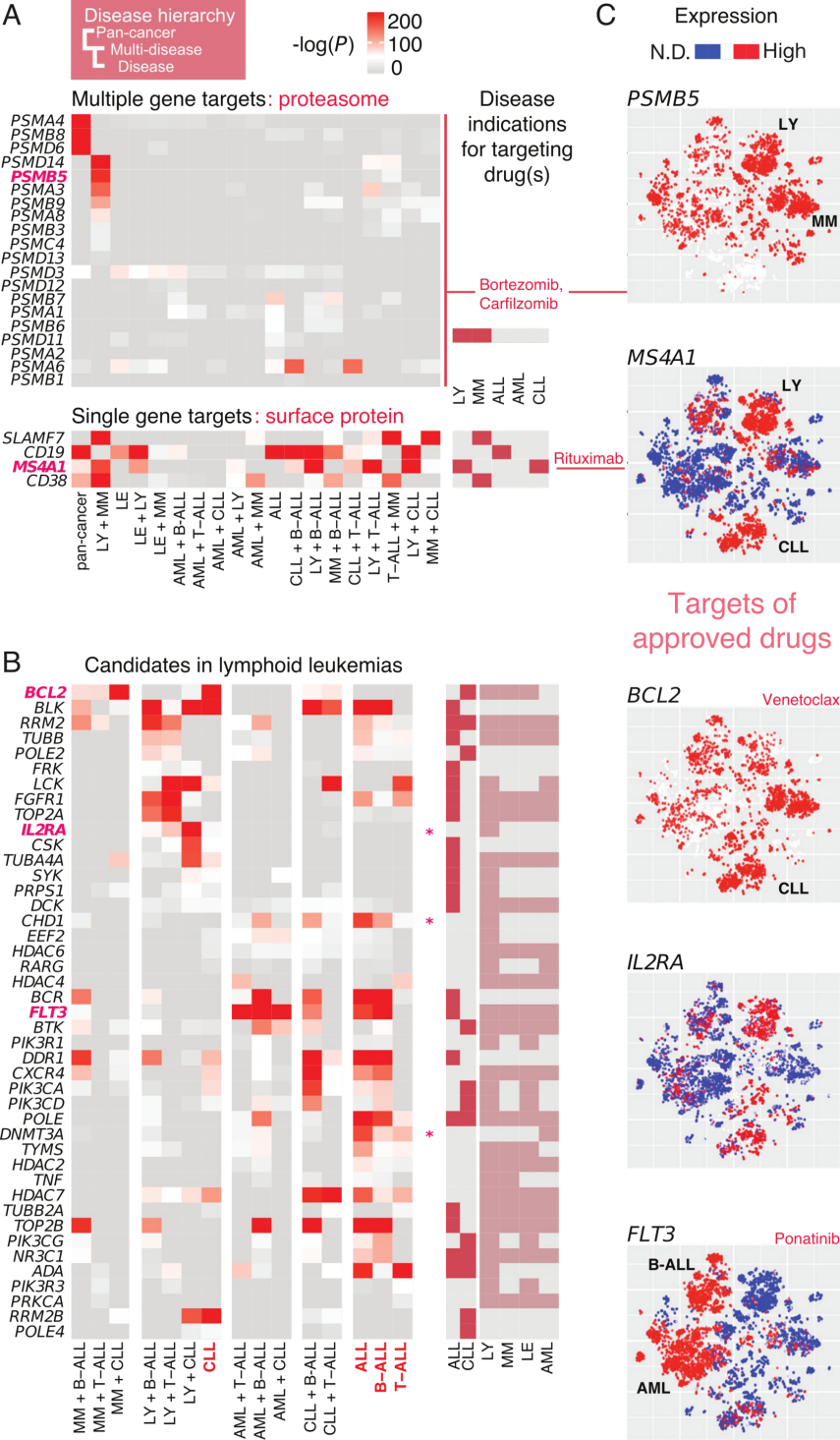
858 Significantly enriched disease clusters are colored on the map based on pan-cancer analysis
859 of epigenetic modifiers (purple: CLL; blue: T-ALL, green: AML cluster 32; pink: pre-B-ALL
860 cluster 28). The expression states of the most significant drug candidates for CLL (*SFMTB1*,
861 *CBX7*, *EZH1*, *EHMT1*, *KMT2B* and *BAZ2A*) are shown (as in **Fig. 2C**) on the right. **B.** The
862 expression level (log₁₀ cpm) and standard deviation (log₂ s.d) of the genes shown in A is
863 indicated on the scatter plot representing independent RNA-seq data⁵² (GSE81274, N=10).

864 **C.** Significance ranking of surface target candidates for pre-B-ALL (x-axis, -log₁₀ *P*-value)
865 are plotted against protein level detection rate. Top candidates (*P*-value < 10⁻²⁵⁰) are
866 indicated next to the plot. **D.** *DPEP1* e-staining is shown as in **A**. **E.** *DPEP1*
867 immunohistochemistry. The sample on the left was interpreted as negative. In the samples in
868 the middle and on the right over 50 percent of the leukemic blasts are showing membranous
869 and cytoplasmic positivity and the staining of the sample was graded as strong positive
870 (FFPE, 40x magnification, Leica DM 3000 microscope, Leica MC190 HD microscope
871 camera, Leica Application Suite software).

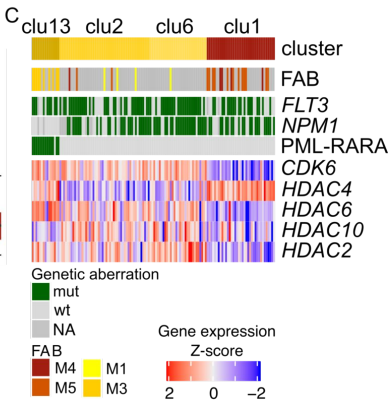
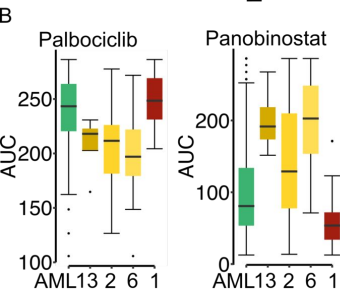
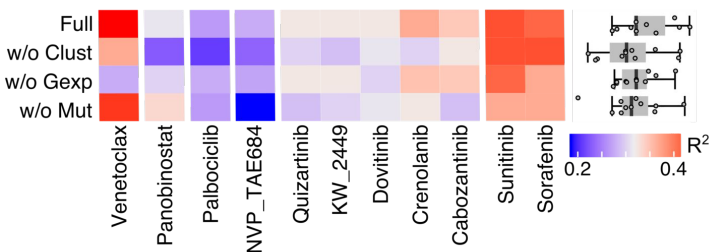
872





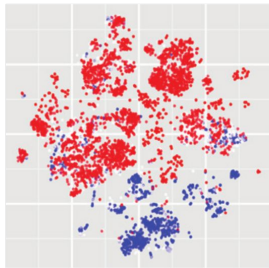


Cluster specificity



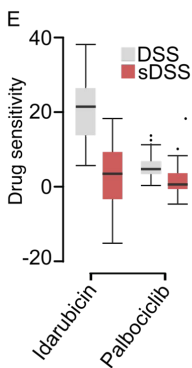
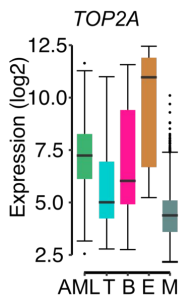
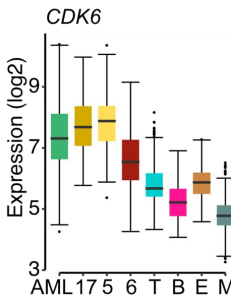
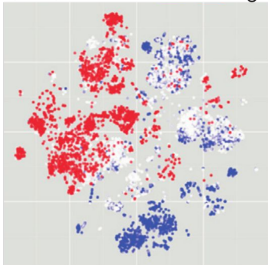
Cancer specificity

TOP2A

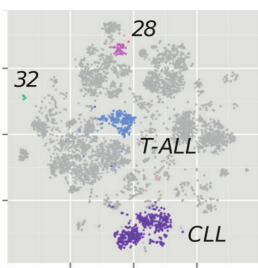


CDK6

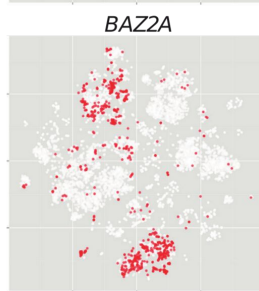
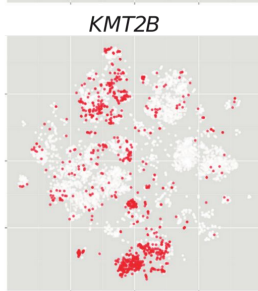
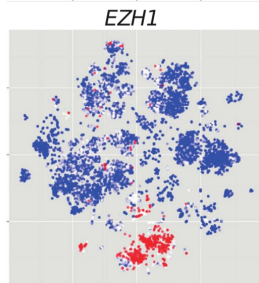
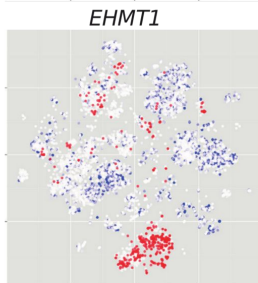
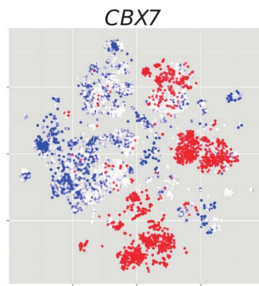
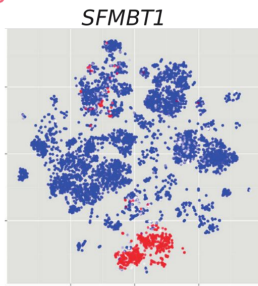
N.D. High



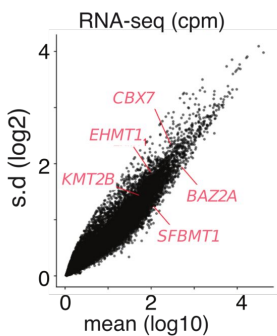
A Epigenetic modifiers



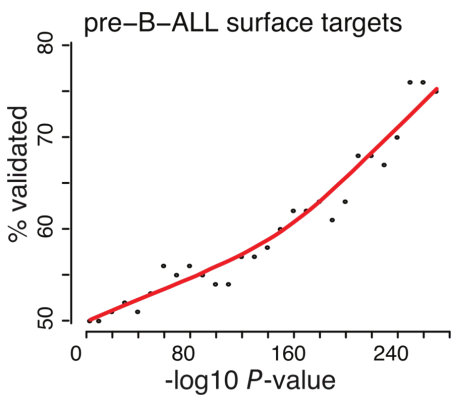
N.D. ■ ■ High



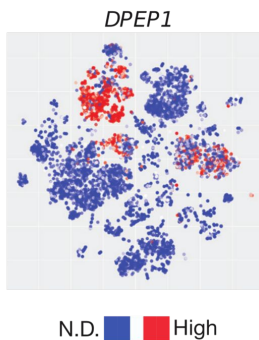
B



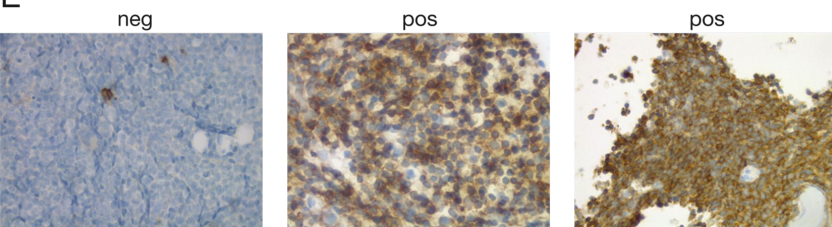
C Surface proteins



D



E



Cancer Research

The Journal of Cancer Research (1916–1930) | The American Journal of Cancer (1931–1940)

Hemap: An interactive online resource for characterizing molecular phenotypes across hematologic malignancies

Petri Pölönen, Juha Mehtonen, Jake Lin, et al.

Cancer Res Published OnlineFirst April 2, 2019.

Updated version	Access the most recent version of this article at: doi: 10.1158/0008-5472.CAN-18-2970
Supplementary Material	Access the most recent supplemental material at: http://cancerres.aacrjournals.org/content/suppl/2019/04/02/0008-5472.CAN-18-2970.DC1
Author Manuscript	Author manuscripts have been peer reviewed and accepted for publication but have not yet been edited.

E-mail alerts	Sign up to receive free email-alerts related to this article or journal.
Reprints and Subscriptions	To order reprints of this article or to subscribe to the journal, contact the AACR Publications Department at pubs@aacr.org .
Permissions	To request permission to re-use all or part of this article, use this link http://cancerres.aacrjournals.org/content/early/2019/04/02/0008-5472.CAN-18-2970 . Click on "Request Permissions" which will take you to the Copyright Clearance Center's (CCC) Rightslink site.